

SYNCHRONIZATION OF KAUFFMAN NETWORKS

Luis G. Morelli and Damián H. Zanette

*Consejo Nacional de Investigaciones Científicas y Técnicas
Centro Atómico Bariloche and Instituto Balseiro, 8400 Bariloche, Río Negro, Argentina*
(October 30, 2018)

We analyze the synchronization transition for a pair of coupled identical Kauffman networks in the chaotic phase. The annealed model for Kauffman networks shows that synchronization appears through a transcritical bifurcation, and provides an approximate description for the whole dynamics of the coupled networks. We show that these analytical predictions are in good agreement with numerical results for sufficiently large networks, and study finite-size effects in detail. Preliminary analytical and numerical results for partially disordered networks are also presented.

PACS: 05.45.Xt, 05.65.+b

I. INTRODUCTION

Synchronization of coupled elements is a form of collective evolution present in a variety of complex real systems and mathematical models. This class of emergent behavior has been observed in biological populations [1], chemical reactions [2], neural networks [3], and human social phenomena [4], among other instances. Models that account for synchronization consider, for example, globally coupled logistic maps [5], chaotic oscillators [6], Hamiltonian systems [7], and formal neural networks [8].

In the usual formulation, two identical dynamical systems whose individual dynamics is governed by the equation $\dot{\mathbf{w}} = \mathbf{F}(\mathbf{w})$ are coupled to each other in the form

$$\dot{\mathbf{w}}_{1,2} = \mathbf{F}(\mathbf{w}_{1,2}) + \epsilon(\mathbf{w}_{2,1} - \mathbf{w}_{1,2}), \quad (1)$$

where ϵ is the coupling parameter. Full synchronization takes place when both systems converge asymptotically to a common trajectory, $\mathbf{w}_1(t) = \mathbf{w}_2(t)$. When the individual dynamics is chaotic—a particularly relevant case in connection with the description of real systems—full synchronization occurs above a critical value ϵ_c of the coupling intensity. This critical point is determined by the competition between chaos and coupling, and can be calculated in terms of the Lyapunov exponent of the individual dynamics [5].

While globally coupled chaotic elements with a few internal variables have been extensively studied, synchronization of spatially extended systems remains quite unexplored. Recently, synchronization has been reported for a system consisting of two coupled complex Ginzburg-Landau equations [9]. Globally coupled neural networks [8], stochastically coupled cellular automata [10–12], and nonidentical complex Ginzburg-Landau systems [13], are

other examples of spatially extended systems that present a critical transition to synchronization.

In this paper we study the synchronization dynamics of two coupled identical Kauffman networks, which are discrete extended dynamical systems with quenched disorder. With respect to previous work on coupled extended systems, the interest of Kauffman networks resides in the fact that the transition to synchronization admits an analytical description which results to be in excellent agreement with numerical simulations. In Sect. II we briefly review the definition of Kauffman networks and the annealed model for the calculation of their overlaps. Next, in Sect. III, we introduce a stochastic coupling mechanism for Kauffman networks and propose an analytical approach in the framework of the annealed model, which identifies the transition to synchronization in our system as a transcritical bifurcation. Section IV, where we report our numerical results, is the core of the present paper. There, we study the effects of spurious synchronization in finite-size networks, consider the application of noise to the system to eliminate such effects, and compare the results with the analytical description. Remnant finite-size effects are numerically quantified and their analytical treatment, which requires a formulation beyond the annealed model, is outlined. In Sect. V we discuss the synchronization transition in some subclasses of Kauffman networks, which may be thought of as interpolations between generic Kauffman networks and ordered cellular automata. Finally, in Sect. VI, our results are summarized and discussed.

II. KAUFFMAN NETWORKS

Kauffman networks, also known as random Boolean networks, were introduced as a model for the problem of cell differentiation [14,15]. Since then, they have been the object of many studies concerning their properties [15–19].

A Kauffman network (KN) is a disordered deterministic dynamical system. It consists of an N -site network, where each site is connected to K randomly chosen sites. The parameter K is known as the *connectivity* of the network. We refer to the set of K sites connected to a given site as its *neighborhood*. The state of each site is given by a Boolean variable $\sigma_i \in \{0, 1\}$, and evolves according to the inputs coming from the neighbor sites. The evolution rule is chosen independently and randomly for each site. To each possible configuration of the neighborhood—

there are 2^K such configurations—an output is assigned, namely, 1 with probability p , or 0 with probability $1 - p$. The parameter $p \in [0, 1]$ is known as the *bias* of the rule. Then, for each variable σ_i we have Boolean functions f_i such that $\sigma_i(t + 1) = f_i[\boldsymbol{\nu}_i(t)]$, where $\boldsymbol{\nu}_i = (\sigma_{i_1}, \dots, \sigma_{i_K})$ is the set of inputs of site i . The state of all sites is updated simultaneously according to the corresponding functions. We can write an evolution equation for the state vector of the network $\boldsymbol{\sigma} = (\sigma_1, \sigma_2, \dots, \sigma_N)$, as

$$\boldsymbol{\sigma}(t + 1) = \mathbf{f}[\boldsymbol{\sigma}(t)], \quad (2)$$

with $\mathbf{f}[\boldsymbol{\sigma}(t)] = (f_1[\boldsymbol{\nu}_1(t)], f_2[\boldsymbol{\nu}_2(t)], \dots, f_N[\boldsymbol{\nu}_N(t)])$.

The K connections and the evolution rule of each site are chosen at the beginning and kept fixed during the evolution. Thus, the disorder is quenched and the dynamics is deterministic. For a finite number of sites N , the number of states in phase space is also finite—it equals 2^N . Then, for any initial condition, the system will eventually fall into a cycle.

In the (p, K) parameter space, Kauffman networks present phases of frozen and chaotic evolution, separated by a critical line. The transition between these phases has been extensively studied, and characterized by means of several order parameters, such as the Hamming distance [16,17] and the stable core size [18]. In most of this work we will deal with the case $p = 1/2$ and $K = 3$, which lies within the chaotic phase.

The annealed model (AM) was introduced to study the evolution of overlaps between states in KNs [16,17]. In this model, the K connections $\{i_1, \dots, i_K\}$ of each site as well as the Boolean functions f_i are randomly changed at each time step. This means that an entirely different realization of the network is used at each step. Note that, while ordinary KNs are deterministic, the annealed model works as a probabilistic automaton. The asymptotic periodic behavior of KNs is absent in the annealed model. The advantage of this model is that it allows for analytical calculations, and it has been shown that its predictions are in good agreement with the behavior of KNs in the limit $N \rightarrow \infty$ [17].

Suppose that we have two identical KNs with the same connections and rules. We feed them with different initial conditions, and let them evolve in time. We define the *overlap* $a(t)$ between the networks as the fraction of homologous sites that are in the same state at time t . In the AM, it is possible to calculate the time evolution of the overlap. At time $t + 1$ the connections and the rules f_i are reassigned, but the same changes are applied to both networks, keeping them identical. The probability for a site having all its inputs coming from sites in the same state in both networks is $a(t)^K$. At the next time step, consequently, such site will be in the same state in both networks, no matter the evolution rule chosen for it. Thus, there is a fraction $a(t)^K$ of homologous sites whose state will coincide at $t + 1$. The remaining $1 - a(t)^K$ sites still have a probability of overlapping. Even if the state of the neighborhoods of a given site are different in

the two networks, it may happen that the evolution rule assigns the same output to them. The probabilities for $f_i(\boldsymbol{\nu}_i^1) = f_i(\boldsymbol{\nu}_i^2) = 0$ and for $f_i(\boldsymbol{\nu}_i^1) = f_i(\boldsymbol{\nu}_i^2) = 1$ are, respectively, $(1 - p)^2$ and p^2 . The overlap at time $t + 1$ is then

$$a(t + 1) = a(t)^K + [1 - a(t)^K] [p^2 + (1 - p)^2]. \quad (3)$$

An alternative way to characterize the difference between two networks is the difference automaton, defined by

$$d_i(t) = \sigma_i^1(t) \oplus \sigma_i^2(t), \quad (4)$$

where \oplus denotes Boolean addition. The density of this automaton is given by

$$D(t) = \frac{1}{N} \sum_{i=1}^N d_i(t), \quad (5)$$

and coincides with the Hamming distance between the networks. Note that $D(t) = 1 - a(t)$ so that, from Eq. (3), we get

$$D(t + 1) = 2p(1 - p) (1 - [1 - D(t)]^K). \quad (6)$$

The Hamming distance has proven to be a suitable order parameter in the study of the synchronization transition in coupled elementary cellular automata [10–12], where the analysis of overlaps between states is a basic tool to define the effects of coupling. In the next section, we adapt the annealed model to the description of coupled KNs.

III. COUPLED KAUFFMAN NETWORKS

A. Stochastic coupling

In order to establish a coupling mechanism between two KNs, we first observe that, due to the discrete nature of KNs, the usual deterministic coupling used for maps [5] cannot be applied here. Consequently, we introduce a form of stochastic coupling between networks as previously done for cellular automata [10], where the continuous parameter q that controls the strength of the coupling is a probability, as explained in the following.

The evolution of the coupled system is implemented by the successive application of two operators. First, the evolution function \mathbf{f} is applied to both networks as if they were not coupled [see Eq. (2)], yielding $\mathbf{f}(\boldsymbol{\sigma}^1)$ and $\mathbf{f}(\boldsymbol{\sigma}^2)$. Next, the stochastic coupling operator \mathcal{S} is applied:

$$\{\boldsymbol{\sigma}^1(t + 1), \boldsymbol{\sigma}^2(t + 1)\} = \mathcal{S}(\mathbf{f}[\boldsymbol{\sigma}^1(t)], \mathbf{f}[\boldsymbol{\sigma}^2(t)]). \quad (7)$$

The operator \mathcal{S} compares the states of the networks site by site. If $\sigma_i^1(t) = \sigma_i^2(t)$ the state of the site is not modified. If, on the other hand, $\sigma_i^1(t) \neq \sigma_i^2(t)$, with probability q the states of the homologous sites in both networks

are set to the same value. This value is chosen among $\sigma_i^1(t)$ and $\sigma_i^2(t)$, with the same probability $1/2$ for each instance. With probability $1 - q$, even if $\sigma_i^1(t) \neq \sigma_i^2(t)$, the coupling does not act, leaving the state of that site unchanged in both networks. We call q the *coupling probability*. The whole evolution can be formally expressed as

$$\{\sigma_i^1, \sigma_i^2\} \rightarrow \begin{cases} \{f_i(\nu_i^1), f_i(\nu_i^2)\} & \text{with probability } 1 - q, \\ \{f_i(\nu_i^1), f_i(\nu_i^1)\} & \text{with probability } q/2, \\ \{f_i(\nu_i^2), f_i(\nu_i^2)\} & \text{with probability } q/2. \end{cases} \quad (8)$$

We stress that we are dealing with two identical extended systems, and that the coupling mechanism connects homologous elements of these two systems, namely, the i th site of network 1 is connected by coupling with the i th site of network 2, as schematically illustrated in Fig. 1. The coupling mechanism defined above is symmetric, since each network may influence the other. It could also be possible to consider a biased, non symmetric coupling, in which one network drives the other [11].

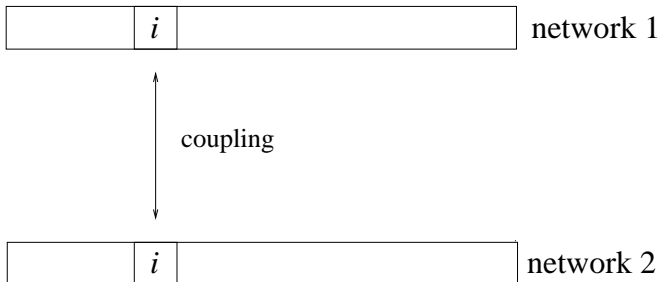


FIG. 1. Schematic representation of the coupling mechanism. Coupling links homologous elements of two extended systems—in this case, two networks. Since coupling is symmetric, each network may act on the other.

For $q = 0$ the two networks are uncoupled, and evolve independently from each other. For $q = 1$, in contrast, the networks synchronize completely at the first time step. From then on, they follow a common trajectory in phase space without further intervention of the coupling mechanism. Our aim in the following is to study the behavior of coupled KNs for intermediate values of the coupling probability, $q \in (0, 1)$.

In the frozen phase, where no damage spreading takes place, an arbitrary small coupling intensity $q > 0$ leads eventually to synchronization. The situation is different in the chaotic phase. There, we find two competing driving forces acting on the coupled system, namely, the chaotic dynamics which induces the separation between two trajectories to grow [15], and the coupling, by which the Hamming distance between the networks decreases. In this paper, we focus attention on the chaotic phase.

B. Annealed model for coupled networks

The annealed model can be used to predict the behavior of the pair of coupled KNs. We recall that the time evolution equation for the Hamming distance in the case of two *free* networks is given by Eq. (6). Now suppose that the Hamming distance of two *coupled* KNs at time t is $D(t)$. The first substep in the dynamics of this system consists of the free evolution of both networks. The Hamming distance after this substep, $D(t + \delta t)$, is therefore given by Eq. (6). At the second substep, coupling acts on the system, and a fraction q of the homologous sites that were in different states are assigned the same value. This leaves a fraction $(1 - q)D(t + \delta t)$ of sites with different states in the two networks. Thus, the evolution of the Hamming distance for coupled networks is given by the map

$$D(t + 1) = F[D(t)] = \varphi(p, q) \left(1 - [1 - D(t)]^K\right), \quad (9)$$

with $\varphi(p, q) = 2p(1 - p)(1 - q)$.

It can be shown that the map (9) has a stable fixed point $D^* > 0$ for $q < q_c$, with

$$q_c = 1 - [2p(1 - p)K]^{-1}. \quad (10)$$

At $q = q_c$ the system undergoes a transcritical bifurcation [20], and $D^* = 0$ becomes a stable fixed point for $q > q_c$. Thus, within the AM approximation, q_c stands for the critical coupling at which synchronization sets on. In this paper we deal mostly with the case $K = 3$, for which the stable equilibrium D^* can be given analytically as a function of the coupling probability q . In this case, in fact, the map is defined by the cubic function $F(x) = \varphi(p, q)x(3 - 3x + x^2)$. The stable Hamming distance is

$$D^*(q) = \begin{cases} \frac{3}{2} - \frac{1}{2} \left[-3 + \frac{4}{\varphi(p, q)}\right]^{1/2} & \text{for } q < q_c, \\ 0 & \text{for } q \geq q_c. \end{cases} \quad (11)$$

Note that near the critical point, $q \lesssim q_c$, this Hamming distance is approximately given by

$$D^*(q) = 6p(1 - p)|q - q_c|. \quad (12)$$

Therefore, the corresponding critical exponent is equal to unity.

For $q \neq q_c$, the Hamming distance approaches $D^*(q)$ exponentially in time. For $q = q_c$, on the other hand, Eq. (9) can be approximately written, for $D(t) \rightarrow 0$, as $D(t + 1) = D(t) - (K - 1)D(t)^2/2$. This implies a power-law decay for long times, $D(t) \sim t^{-1}$. In the next section, we compare these analytical results with those of extensive numerical simulations.

IV. NUMERICAL RESULTS

We have performed numerical simulations of pairs of KNs coupled under the scheme presented above. The results reported in this section correspond to the case of $p = 1/2$ and $K = 3$. We have recorded the time evolution of the Hamming distance, performing averages over r realizations of N -site networks. The number of realizations is chosen in such a way that, for different values of N , $rN \geq 10^6$. In a typical realization, we start with two identical networks with different random initial conditions. For each realization, new connections and local functions are chosen. The networks are allowed to evolve freely, without coupling, for a transient time τ of, typically, 10^3 steps. This is done for the networks to reach their asymptotic dynamics before coupling is allowed to act. After this transient, we turn the coupling on, reset the time to zero, and start measuring $D(t)$.

In Fig. 2 we show the time evolution of the Hamming distance $D(t)$ for different values of the coupling parameter q . The values of q have been chosen to display the three typical behaviors, namely, synchronization for $q > q_c$, critical decay for $q \approx q_c$, and convergence to a finite distance for $q < q_c$.

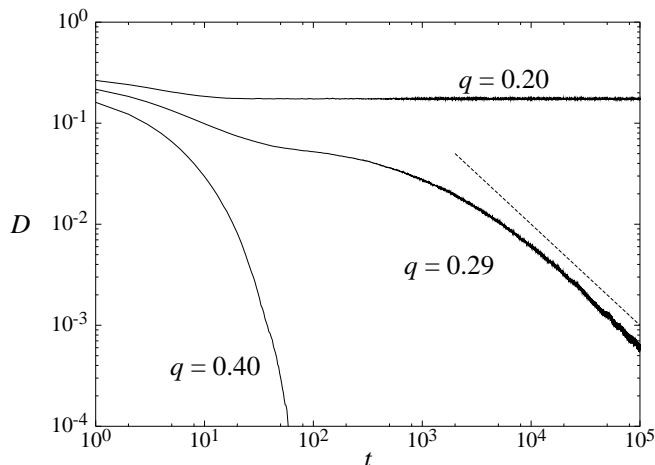


FIG. 2. Hamming distance as a function of time for 10^3 -site networks and three coupling probabilities q , averaged over 10^4 realizations. The dashed line, of slope -1 , is to be compared with the power-law decay observed near the critical coupling.

For the present values of p and K , the annealed model predicts a critical coupling probability $q_c = 1/3$ [cf. Eq. (10)]. It is however clear from Fig. 2 that the power-law decay in $D(t)$ is observed for a lower coupling, $q = 0.29$. Simulations of the same networks with $q = 1/3$, on the other hand, always lead to synchronization. In fact, the annealed model is expected to provide a good approximation to our system in the limit $N \rightarrow \infty$ [17]. Figure 3 shows the time evolution of the Hamming distance for a fixed coupling probability, $q = 0.29$, and several values of N . The AM prediction from Eq. (9) is also shown. The strong dependence with the size of the network is appar-

ent. In particular, we find that for this coupling strength 10^3 -site networks synchronize whereas 10^4 -site networks do not. The AM result gives a good description for the case of $N = 10^4$.

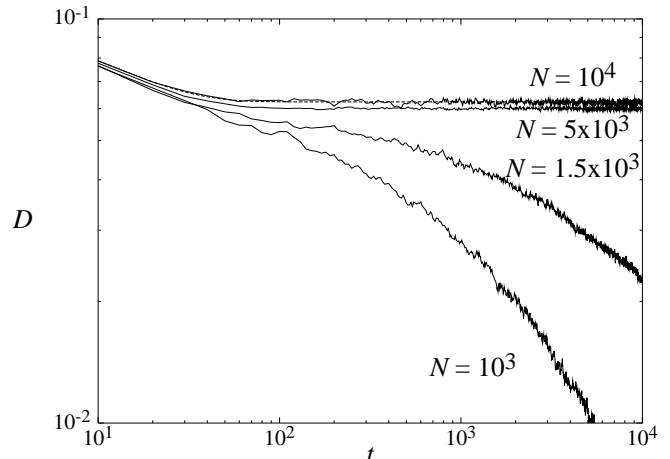


FIG. 3. Hamming distance as a function of time for several network sizes N , and fixed coupling probability $q = 0.29$. Averages were done over 10^3 realizations for $N < 10^4$, and over 10^2 realizations for $N = 10^4$. The dashed curve stands for the annealed model prediction.

The dependence of $D(t)$ on the size of the system can be partially ascribed to the effect of *spurious synchronization*. Because of the discrete nature of KNs, two finite-size networks can be brought to the same state by a fluctuation caused by the stochastic coupling. In such case, the two networks will remain synchronized from then on. This event is more frequent for small networks, where the relative size of fluctuations increases. Near the critical point, furthermore, where the Hamming distance vanishes asymptotically, the effect of fluctuations is strongly enhanced. The net result of spurious synchronization is that the effective critical coupling for finite-size networks shifts to lower values as N decreases. As a consequence, the average Hamming distance in our simulations may vanish even for coupling probabilities below q_c , as illustrated in Figs. 2 and 3.

Spurious synchronization can be avoided by adding noise to the system. Such strategy has already been adopted in this field, specifically, in the study of globally coupled chaotic maps [21,22], to prevent synchronization due to round-off errors in computer simulations. We implement the addition of noise as a new substep in the dynamics of our system. After the evolution and coupling substeps, we flip the state of each site in one of the networks with a small probability η . Figure 4 illustrates the effect of noise in the evolution of $D(t)$ for $q = 0.29$ and $N = 10^3$. For this coupling intensity, where the consequences of spurious synchronization are vast, the behavior of the Hamming distance with and without noise changes drastically.

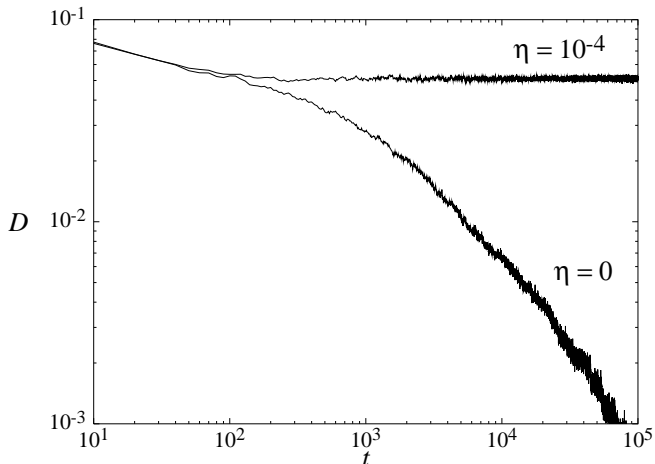


FIG. 4. Hamming distance as a function of time for 10^3 -site networks with $q = 0.29$ and two values of the noise intensity η , averaged over 10^3 realizations. The effects of spurious synchronization for $\eta = 0$ are apparent.

Note that noise eliminates spurious synchronization for $q < q_c$, but also prevents the KNs to exactly synchronize even for $q > q_c$. Therefore, the critical behavior that characterizes the synchronization transition in the absence of noise disappears as noise is added, and is recovered only for $\eta \rightarrow 0$ (but $\eta \neq 0$). The effect of noise can be straightforwardly incorporated to the AM approximation.

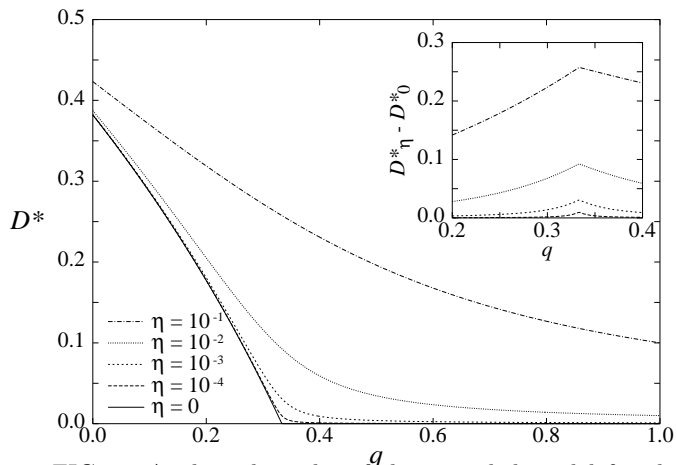


FIG. 5. Analytical results of the annealed model for the asymptotic Hamming distance D_η^* , for different noise intensities η . The insert shows the deviation $D_\eta^* - D_0^*$ from the distance in the absence of noise.

The map that gives the time evolution of the Hamming distance is now

$$D(t+1) = (1-\eta)F[D(t)] + \eta(1-F[D(t)]), \quad (13)$$

with $F[D(t)]$ given by Eq. (9). As for the model without noise, for $K = 3$ it is possible to analytically find the asymptotic distance D_η^* predicted by Eq. (13). Figure

5 shows D_η^* as a function of the coupling probability q for various noise intensities. Note the approximation to the critical behavior as $\eta \rightarrow 0$. The insert displays the difference between D_η^* and the asymptotic distance in the absence of noise as a function of q .

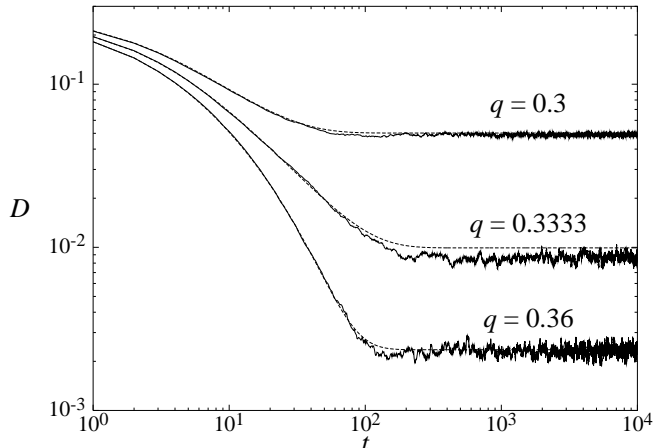


FIG. 6. Hamming distance as a function of time for 10^4 -site networks and three values of the coupling probability q , averaged over 10^2 realizations. The noise intensity is $\eta = 10^{-4}$.

In Fig. 6, we compare the prediction of Eq. (13) with numerical results for the Hamming distance of two coupled 10^4 -site KNs with noise intensity $\eta = 10^{-4}$, for three values of the coupling intensity. The agreement is excellent during the transients, but some noticeable discrepancies persist in the asymptotic value, especially, for $q \approx q_c$.

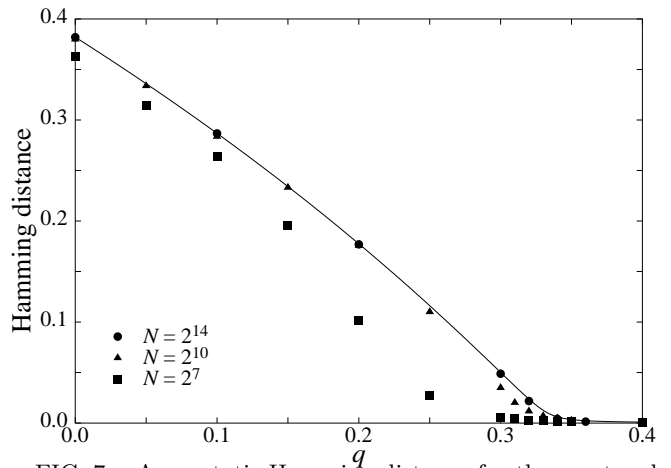


FIG. 7. Asymptotic Hamming distance for three network sizes N , averaged over 5×10^3 time steps and 10^3 realizations. The noise intensity is $\eta = 10^{-4}$. The curve corresponds to the AM prediction.

To study such discrepancies in detail, and thus test the AM results, we compute from our numerical simulations the average asymptotic value of $D(t)$, defined as

$$\langle D \rangle = \frac{1}{T} \sum_{t=t_0}^{t_0+T} D(t). \quad (14)$$

Averages are performed over a time span T of 5×10^3 time steps, when the asymptotic regime of the coupled system has been reached, i.e. for sufficiently large values of t_0 . As above, we choose $\eta = 10^{-4}$, and determine $\langle D \rangle$ for several values of N . Results for $N = 2^7, 2^{10}$, and 2^{14} are presented in Fig. 7. The AM prediction for this value of η is also shown, as a curve. We see that the AM results systematically overestimate the values of $\langle D \rangle$, and that the agreement improves for larger values of N . Therefore, even when noise has been added to avoid spurious synchronization, finite-size effects persist.

These remanent finite-size effects are measured by the difference $\delta D^* = D_\eta^* - \langle D \rangle$ between the AM prediction and the numerical average defined in Eq. (14). In Fig. 8 we plot δD^* as a function of N for different coupling intensities. The insert shows D_η^* and $\langle D \rangle$ as a function of N for the same values of q . There are two well-differentiated regimes in the size dependence of δD^* . For small N , the deviation between the AM estimate and numerical results is practically constant. For large values of N the deviation decreases, seemingly as a power-law, $\delta D^* \sim N^{-z}$. Least-square fits for $N > 10^2$ yield $z = 1.1 \pm 0.2$ for the exponent.

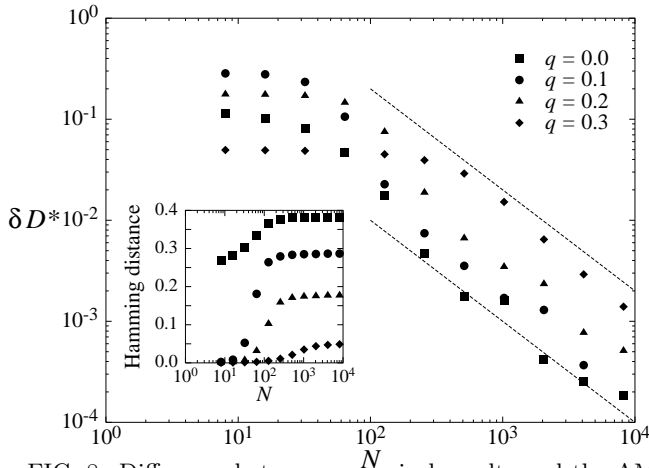


FIG. 8. Difference between numerical results and the AM prediction for the asymptotic Hamming distance as a function of size, for four coupling probabilities q . The dashed lines have slope -1 . The insert shows the asymptotic Hamming distance in semilogarithmic scale, to appreciate the behavior for small values of N .

To find an explanation for these finite size effects, it is necessary to go beyond the annealed approximation. In the following, we outline an approach to the calculation of the Hamming distance based on statistical averages over states of the KNs. The density of a state $\sigma = (\sigma_1, \dots, \sigma_N)$ of a single KN is defined as

$$\rho(\sigma) = \frac{1}{N} \sum_{i=1}^N \sigma_i \quad (15)$$

[cf. Eq. (5)], whereas the distance between two states σ and σ' reads

$$D(\sigma, \sigma') = \frac{1}{N} \sum_{i=1}^N (\sigma_i - \sigma'_i)^2. \quad (16)$$

For fixed p, K and N , a realization R of the network is defined by the connections and the local rules. We define Ω_R as the set of all the states visited by the KN for this realization, at asymptotically large times and from all the possible initial conditions. In other words, the set Ω_R contains all the states that belong to the limit cycles of the dynamics. It is possible to introduce a probability distribution $\mathcal{P}_R(\sigma)$ over Ω_R , given by the frequency with which a given state σ is visited at asymptotically large times averaged over all initial conditions. Averages over Ω_R will be computed with this distribution. For instance, the average of the density ρ is

$$d_R = \langle \rho(\sigma) \rangle_{\Omega_R} = \sum_{\sigma \in \Omega_R} \mathcal{P}_R(\sigma) \rho(\sigma). \quad (17)$$

The average of the distance between two states, Eq. (16), can be written as

$$\langle D(\sigma, \sigma') \rangle_{\Omega_R} = 2d_R(1 - d_R) - \frac{2}{N} \sum_{i=1}^N \xi_i^2, \quad (18)$$

where $\xi_i = \langle \sigma_i \rangle_{\Omega_R} - d_R = \langle \sigma'_i \rangle_{\Omega_R} - d_R$. Here, we have assumed that the occurrence of states σ and σ' are probabilistically uncorrelated.

The quantities ξ_i measure, for each realization of the network, the average deviation of the state of each site from the average density d_R over the whole network. Let us introduce the distribution $\Gamma_R(\xi)$ as the fraction of sites in the KN with deviation ξ for a specific realization R . Unfortunately, the explicit form of $\Gamma_R(\xi)$ is not known. It is however known that this is a nontrivial distribution, in particular, due to existence of the so-called stable core [18]. The stable core is a set of sites that have always the same asymptotic, fixed states, irrespectively of the initial condition. For these sites, $\langle \sigma_i \rangle_{\Omega_R} = 0$ or 1 , so that the deviations ξ_i adopt their extremal values, $\xi_i = -d_R$ or $1 - d_R$, respectively. Using the distribution $\Gamma_R(\xi)$ to replace the sum in Eq. (18) by an integral, we have

$$\langle D(\sigma, \sigma') \rangle_{\Omega_R} = 2d_R(1 - d_R) - 2 \int_{-d_R}^{1-d_R} \Gamma_R(\xi) \xi^2 d\xi. \quad (19)$$

Now, analytical results on the size of the stable core [18] suggest that, as $N \rightarrow \infty$, $\Gamma_R(\xi)$ approaches an asymptotic profile $\Gamma(\xi)$ which depends on p and K , but becomes

independent of the specific realization of the network. For large sizes, we may assume a dependence of the form

$$\Gamma_R(\xi) \approx \Gamma(\xi) - N^{-1}\Gamma'_R(\xi), \quad (20)$$

where Γ'_R is the first (analytical) correction due to finite sizes. Within these assumptions, Eq. (19) takes the form

$$\langle D(\boldsymbol{\sigma}, \boldsymbol{\sigma}') \rangle_{\Omega_R} = D_0 - \frac{2}{N} \int_{-d_R}^{1-d_R} \Gamma'_R(\xi) \xi^2 d\xi, \quad (21)$$

where

$$D_0 = 2d_R(1 - d_R) - 2 \int_{-d_R}^{1-d_R} \Gamma(\xi) \xi^2 d\xi \quad (22)$$

is the asymptotic distance for $N \rightarrow \infty$.

We now associate $\langle D(\boldsymbol{\sigma}, \boldsymbol{\sigma}') \rangle_{\Omega_R}$ with the distance between the states of two coupled KNs at a given (long) time. Indeed, in our system both networks have the same connections and rules, and correspond therefore to the same realization R of the network. According to the definition (4) and (5), after an average over realizations of the network for fixed p , K , and N is performed, the distance $\langle D(\boldsymbol{\sigma}, \boldsymbol{\sigma}') \rangle_{\Omega_R}$ coincides with the Hamming distance $\langle D \rangle$, Eq. (14), considered above. In Eq. (21), thus, D_0 should correspond to the Hamming distance predicted by the AM approximation, valid for $N \rightarrow \infty$, and the first correction to the AM estimate is given by the additional term. As found from our simulations, this term depends on the network size as N^{-1} . The ansatz (20) is therefore supported by numerical results. Note that these conclusions are independent of the strength of coupling, measured by the probability q , since the only effect of the coupling dynamics in connection with the above analysis is to change the set of asymptotic states Ω_R and the profile of the distribution $\Gamma_R(\xi)$.

V. DISORDERED CELLULAR AUTOMATA AND PARTIALLY ORDERED NETWORKS

According to the results reported in the previous sections, the synchronization transition of stochastically coupled KNs on the one hand, and of stochastically coupled elementary cellular automata (ECA, [23]) on the other, are qualitatively different. Namely, they belong to different universality classes. Whereas we have found that synchronization in KNs appears through a transcritical bifurcation—with a critical exponent equal to unity for the asymptotic Hamming distance—the corresponding transition in ECA has been shown to exhibit nontrivial exponents [10], which seem to suggest that it belongs to the universality class of directed percolation [12]. It is therefore relevant to study a third class of systems, intermediate between ECA and generic KNs.

In a generic KN there are two sources of disorder. We have the network topology, determined by the random

choice of connections, and the local evolution rules, which are also chosen at random. On the other hand, in cellular automata both the topology and the dynamical rules are fully homogeneous. ECA can indeed be interpreted as a very special subclass of KNs with $K = 3$, where the choice of dynamical rules and connections is deterministic. In order to distinguish between the effects of disorder in the topology and in the dynamics on the synchronization transition, we consider now the subclass of KNs where the connections are still chosen at random but the local rule is the same for all sites. We refer to these networks as disordered cellular automata (DCA).

We focus here on the elementary rule 22, which exhibits chaotic evolution [23]. This rule is defined by the Boolean function $f(\{0, 0, 1\}) = f(\{0, 1, 0\}) = f(\{1, 0, 0\}) = 1$ and $f = 0$ for the remaining five possible neighborhoods (see Table I). Thus, the bias for rule 22 is $p = 3/8$. This DCA, however, cannot be thought of as a KN with $p = 3/8$. In a generic KN with this bias, in fact, the local evolution could be substantially different from the behavior of rule 22. In particular, the dynamics at some sites may be governed by nonchaotic rules, giving rise to sensible differences in the global behavior. This is clearly illustrated, for instance, by a measurement of the asymptotic density of a rule-22 DCA, which yields $d \approx 0.423$, instead of $d = p = 0.375$.

The formulation of an annealed model of DCA requires a different approach, in order to account for the homogeneity of the dynamical rules. We define the AM by reassigning all the connections at each time step, but keeping the functions $f_i = f$ fixed. Suppose that we have two networks with overlap $a(t)$. The probability for a site to have exactly $K - l$ of its reassigned inputs coming from homologous sites in the same state is

$$p_l(t) = \binom{K}{l} a(t)^{K-l} [1 - a(t)]^l. \quad (23)$$

We introduce the quantity A_l as the probability for two homologous sites having all but l inputs coming from homologous sites in the same state to give the same output. The overlap at time $t + 1$ is then given by

$$a(t + 1) = \sum_{l=0}^K A_l p_l(t). \quad (24)$$

The quantities A_l depend on the evolution rule, and their value is fixed. They can be evaluated within some approximations, as shown in the Appendix. Note that $A_0 = 1$ because, no matter the rule, if the inputs are all equal the outputs will coincide. In the annealed model for KNs we had $A_0 = 1$ and $A_l = p^2 + (1 - p)^2$ for $l = 1, \dots, K$. For $K = 3$ the map for the Hamming distance can be casted into the form

$$D(t + 1) = B_1 D(t) + B_2 D(t)^2 + B_3 D(t)^3, \quad (25)$$

with $B_1 = 3(1 - A_1)$, $B_2 = 3(2A_1 - A_2 - 1)$, $B_3 = -3A_1 + 3A_2 - A_3 + 1$. Coupling enters then the for-

mulation exactly as in Eq. (9), as an additional factor $1 - q$ in the evolution of $D(t)$.

In Fig. 9, the curve stands for the asymptotic value D^* as a function of the coupling probability predicted from Eq. (25) for rule 22. The prediction is qualitatively similar to that for KNs, in particular, in the region close to the synchronization transition. Numerical results on DCA with rule 22 for $N = 2^{11}$ are also shown in Fig. 9. To avoid spurious synchronization, a small amount of noise, $\eta = 10^{-4}$, has been added. The agreement with the AM is reasonably good, though some systematic deviations are clearly visible in the zone of the transition. As before, these deviations may be attributed to finite-size effects.

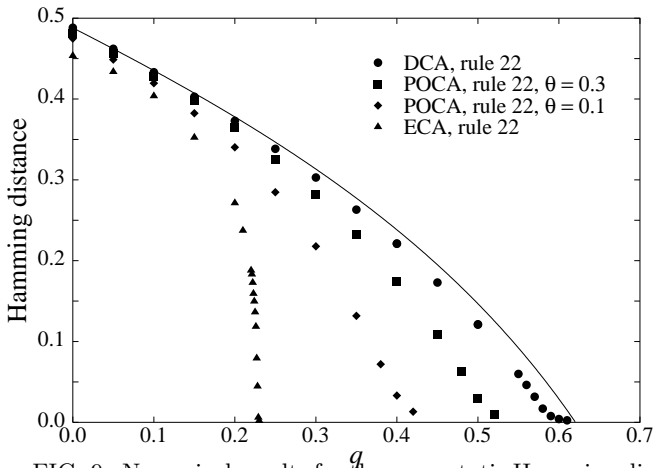


FIG. 9. Numerical results for the asymptotic Hamming distance in coupled 2^{11} -site disordered cellular automata with the evolution rule 22, for different amounts of disorder. The curve stands for the annealed model prediction for DCA.

Finally, as an interpolation between DCA and ECA we consider partially ordered topologies (POCA), constructed in the following way. We start with an N -site ECA, which consists of a one-dimensional array where each site is connected to itself and to its two nearest neighbors. Then, for each site, each neighbor is redrawn at random from the whole network with probability θ . With the complementary probability, $1 - \theta$, the neighbor is preserved. The resulting topological structure of connections is analogous to that of small-world networks [24]. For $\theta = 1$, we recover the DCA networks discussed above. Results of numerical simulations on POCA with rule 22 are shown in Fig. 9 for $\theta = 0.1$ and $\theta = 0.3$. Data for ECA with rule 22 ($\theta = 0$) are also shown. We see that, in spite of the relatively low values of θ , the asymptotic Hamming distance of POCA depends on the coupling probability q in a way qualitatively similar to that of KNs. In particular, it does not exhibit the abrupt dependence on q observed in ECA near the critical point. This would be in agreement with the crossover scenario in small-world networks [25], where it is known that even small amounts of disorder induce behaviors which already

resemble that of fully random structures.

VI. SUMMARY AND DISCUSSION

We have studied the behavior of two Kauffman networks interacting through a form of symmetric stochastic coupling. As for many other localized or extended, random or deterministic, coupled dynamical systems [5–12], we have found that coupled Kauffman networks can synchronize their evolution if coupling is strong enough. In our case, there is a critical value of the coupling probability q beyond which the two networks converge to the same trajectory as time elapses.

In contrast with the situation encountered for other extended systems [8–13], however, for Kauffman networks it has been possible to give an analytical description of the synchronization transition, in excellent agreement with numerical results for large-size systems. This formulation is provided by an extension of the so-called annealed model [16,17] to the system of coupled networks. The model gives the evolution of the overlap between the two networks—or, in other words, of their Hamming distance—and makes it possible to evaluate its asymptotic value. The asymptotic Hamming distance D^* is used as an order parameter for the synchronization transition. For coupled Kauffman networks in the chaotic phase, the annealed model predicts the existence of a critical coupling probability q_c , such that D^* is finite for $q < q_c$ and vanishes for $q > q_c$. At the critical point, $D^* \sim |q - q_c|$, and the transition has the character of a transcritical bifurcation.

The transition predicted by the annealed model is qualitatively different from that observed in the deterministic version of this kind of systems, more specifically, in cellular automata. For elementary cellular automata, in fact, the critical behavior of the Hamming distance exhibits nontrivial exponents [10]. It has been suggested that, at least for some evolution rules, the synchronization transition in cellular automata belongs to the class of directed percolation [12]. On the other hand, by analogy with the problem of damage spreading, synchronization in Kauffman networks could belong to the class of directed percolation in disordered systems [26].

Results from extensive numerical simulations of relatively large networks (10^4 sites), performed for Kauffman networks in the chaotic regime ($p = 1/2$, $K = 3$), are in good agreement with the predictions of the annealed model both in the temporal evolution and in the asymptotic behavior of the system. However, for small networks some systematic departures from the analytical results are apparent. These deviations can be partially explained taking into account the occasional events of spurious synchronization for $q < q_c$, due to the effect of suitably large fluctuations on our discrete finite-size system. The effect of these fluctuations becomes more important as the coupling probability approaches its critical

value. In any case, spurious synchronization can be successfully eliminated by adding a small amount of noise to the dynamics. Moreover, noise can also be encompassed into the annealed model. We have introduced noise in the simulations and observed that remanent finite-size effects persist. These must now be ascribed to the failure of the annealed model in describing finite networks. By means of a more detailed statistical description of the overlaps between networks, in fact, we have been able to account for such remanent effects, also explaining the dependence of the deviation from the annealed model on the network size.

Finally, we have presented preliminary numerical results on disordered and partially ordered stochastically coupled cellular automata. These systems can be seen as providing a kind of interpolation between Kauffman networks, with their completely random connections and dynamical rules, and cellular automata, which are fully ordered. In the case of disordered networks with the same evolution rule on all the sites, it is possible to extend the annealed model, which predicts the same class of synchronization transition as for Kauffman networks. Numerical simulations agree with these predictions. Increasing the order in the connections by means of a scheme analogous to the construction of a small-world network [24], we have also considered partially disordered structures. Even for small amounts of structural disorder, the behavior associated with the synchronization transition seems to resemble that of Kauffman networks more than that of cellular automata. This leads us to conjecture that the synchronization transition of partially disordered automata is in the same universality class as for coupled Kauffman networks. Nevertheless, further extensive simulations and a careful determination of the critical exponents are necessary to draw any conclusions on this point.

ACKNOWLEDGMENT

This work has been partially carried out at the Abdus Salam Centre for Theoretical Physics (Trieste, Italy). The authors thank the Centre for hospitality.

APPENDIX: COEFFICIENTS FOR THE ANNEALED MODEL

In this Appendix we illustrate the computation of the coefficients A_l in Eq. (24) with an explicit example. We recall that A_l is defined as the probability for two homologous sites having all but l inputs coming from homologous sites in the same state to give the same output.

Let us assume that the frequency with which a given neighborhood appears in a state of the whole network is fully determined by the density d of the state. Namely,

we neglect the correlations between neighborhood frequencies, associated with the spatial patterns generated by the dynamics. For $K = 3$, there are eight possible neighborhoods, which we label from 0 to 7 as shown in Table I. Within the above assumption, the frequency p_i of each neighborhood i can be estimated in terms of the density d as

$$\begin{aligned} p_0 &= (1-d)^3, \\ p_1 &= p_2 = p_4 = d(1-d)^2, \\ p_3 &= p_5 = p_6 = d^2(1-d), \\ p_7 &= d^3. \end{aligned} \quad (\text{A1})$$

Moreover, we note that the density d can in turn be written in terms of the frequencies p_i of neighborhoods with nonzero output. For rule 22 these neighborhoods are $\{1, 0, 0\}$, $\{0, 1, 0\}$ and $\{0, 0, 1\}$ (see Table I), so that we have

$$d = p_1 + p_2 + p_4. \quad (\text{A2})$$

Combining Eqs. (A1) and (A2) yields $d = 1 - \sqrt{3}/3 \approx 0.423$, which agrees with the numerical measurement reported in Sect. V. The corresponding values of the frequencies p_i are shown in Table I. They are in very good agreement with the values obtained from numerical simulations, also shown in the table. This supports our above assumption of uncorrelated neighborhood frequencies.

Once the frequencies p_i are known, we are able to calculate the coefficients A_l . As a specific example, we discuss A_3 . By definition, this is the probability for two homologous sites having all but 3 inputs coming from homologous sites in the same state to give the same output. Thus, we are in the case where the two neighborhoods have all the homologous sites in different states. The pairs of neighborhoods that satisfy this condition are $\{0, 7\}$, $\{1, 6\}$, $\{2, 5\}$, and $\{3, 4\}$. Among them, however, only the pair $\{0, 7\}$ has the same output for both neighborhoods (see Table I). The coefficient A_3 is therefore given by

$$A_3 = \frac{p_0 p_7}{p_0 p_7 + p_1 p_6 + p_2 p_5 + p_3 p_4} = \frac{1}{4}. \quad (\text{A3})$$

The computation of the other coefficients is accomplished in a similar way, yielding $A_1 = 4(19 - 8\sqrt{3})/169$ and $A_2 = (9 + \sqrt{3})/13$. Moreover, $A_0 = 1$.

-
- [1] A.T. Winfree, *The Geometry of Biological Time* (Springer, Berlin, 1980).
 - [2] N. Khrustova, G. Vesper, A. Mikhailov, and R. Imbihl, *Phys. Rev. Lett.* **75**, 3564 (1995).
 - [3] H. D. Abarbanel, M. I. Rabinovich, A. Selverston, M. V. Bazhenov, R. Huerta, M. M. Sushchik, and L. L. Rubchinskii, *Usp. Fiz. Nauk.* **166**, 363 (1996) [*Phys. Usp.* **39**, 337 (1996)].

- [4] Z. Néda, E. Ravasz, T. Vicsek, Y. Brechet, and A. L. Barabási, Phys. Rev E **61**, 6987 (2000).
- [5] K. Kaneko, Physica D **23**, 436 (1986); *ibid.* **37**, 60 (1989); *ibid.* **54**, 5 (1991).
- [6] J. F. Heagy, T. L. Carrol, and L. M. Pecora, Phys. Rev. E **50**, 1874 (1994).
- [7] D. H. Zanette and A. S. Mikhailov, Phys. Lett. A **235**, 135 (1997); A. Hampton and D. H. Zanette, Phys. Rev. Lett. **83**, 2179 (1999).
- [8] D. H. Zanette and A. S. Mikhailov, Phys. Rev. E **58**, 872 (1998).
- [9] A. Amengual, E. Hernández-García, R. Montagne, and M. San Miguel, Phys. Rev. Lett. **78**, 4379 (1997).
- [10] L. G. Morelli and D. H. Zanette, Phys. Rev. E **58**, R8 (1998).
- [11] F. Bagnoli and R. Rechtman, Phys. Rev. E **59**, R1307 (1999).
- [12] P. Grassberger, Phys. Rev. E **59**, R2520 (1999).
- [13] S. Boccaletti, J. Bragard, F. T. Arecchi, and H. Mancini, Phys. Rev. Lett. **83**, 536 (1999).
- [14] S. A. Kauffman, J. Theor. Biol. **22**, 437 (1969); Nature **244**, 177 (1969).
- [15] S.A. Kauffman, *The Origins of Order* (Oxford University Press, Cambridge, 1993).
- [16] B. Derrida and Y. Pomeau, Europhys. Lett. **1**, 45 (1986).
- [17] B. Derrida and G. Weisbuch, J. Physique **47**, 1297 (1986).
- [18] H. Flyvbjerg, J. Phys. A **21**, L955 (1988).
- [19] U. Bastolla and G. Parisi, Physica D **98**, 1 (1996); *ibid.* **115**, 203 (1998); *ibid.* **115**, 219 (1998).
- [20] K. T. Alliwod, T. D. Sauer, and J. A. Yorke, *Chaos. An Introduction to Dynamical Systems* (Springer, New York, 1997).
- [21] K. Kaneko, Physica D **124**, 322 (1998).
- [22] S. C. Manrubia and A. S. Mikhailov, Europhys. Lett. **50**, 580 (2000).
- [23] S. Wolfram, Rev. Mod. Phys. **55**, 601 (1983).
- [24] D. J. Watts and S. H. Strogatz, Nature **393**, 440 (1998).
- [25] M. Barthélémy sand L. A. N. Amaral, Phys. Rev. Lett. **82**, 3180 (1999).
- [26] P. Grassberger, J. Stat. Phys. **79**, 13 (1995).

label	neighborhood	output	$p_{\text{numerical}}$	$p_{\text{analytical}}$
0	{0, 0, 0}	0	0.19350	0.19294
1	{0, 0, 1}	1	0.14075	0.14096
2	{0, 1, 0}	1	0.14071	0.14096
3	{0, 1, 1}	0	0.10287	0.10298
4	{1, 0, 0}	1	0.14079	0.14096
5	{1, 0, 1}	0	0.10290	0.10298
6	{1, 1, 0}	0	0.10289	0.10298
7	{1, 1, 1}	0	0.07559	0.07524

TABLE I. Cellular automata neighborhoods and their outputs for the evolution rule 22. The frequencies p for each neighborhood obtained from numerical results and from the analytical approximation used in the Appendix are also quoted.